Am J Physiol Heart Circ Physiol 288: H2588–H2593, 2005.
First published January 21, 2005; doi:10.1152/ajpheart.01060.2004.

Impaired resting perfusion in viable myocardium distal to chronic coronary stenosis in rats

Christiane Waller,[1] Tobias Engelhorn,[3] Karl-Heinz Hiller,[2] Gerd Heusch,[4] Georg Ertl,[1] Wolfgang Rudolf Bauer,[1] and Rainer Schulz[4]

[1]*Medizinische Universitätsklinik and* [2]*Physikalisches Institut, Würzburg; and* [3]*Abteilung für Neuroradiologie and* [4]*Institut für Pathophysiologie, Universität Essen, Essen, Germany*

Submitted 15 October 2004; accepted in final form 13 December 2004

Waller, Christiane, Tobias Engelhorn, Karl-Heinz Hiller, Gerd Heusch, Georg Ertl, Wolfgang Rudolf Bauer, and Rainer Schulz. Impaired resting perfusion in viable myocardium distal to chronic coronary stenosis in rats. *Am J Physiol Heart Circ Physiol* 288: H2588–H2593, 2005. First published January 21, 2005; doi:10.1152/ajpheart.01060.2004.—Chronic coronary artery stenosis results in patchy necrosis in the dependent myocardium and impairs global and regional left ventricular (LV) function in rats in vivo. The aim of the present study was to compare regional myocardial blood flow (RMBF) and function (F) in poststenotic myocardium by using magnetic resonance imaging (MRI) and to compare MRI blood flow changes to histological alterations to assess whether RMBF in the viable poststenotic tissue remains normal. MRI was performed in 11 anesthetized Wistar rats with 2-wk stenosis of the left coronary artery. Postmortem, the extent of fibrotic tissue was quantified. Poststenotic RMBF was significantly reduced to 2.21 ± 0.30 $ml \cdot g^{-1} \cdot min^{-1}$ compared with RMBF in the remote myocardium (4.05 ± 0.50 $ml \cdot g^{-1} \cdot min^{-1}$). A significant relationship between the poststenotic RMBF (%remote area) and the poststenotic F (%remote myocardium) was calculated ($r = 0.61$, $P < 0.05$). Assuming perfusion in scar tissue to be 32 ± 5% of perfusion of remote myocardium, as measured in five additional rats, and that in remote myocardium to be 114 ± 25% of that in normal myocardium, as assessed in five sham rats, the calculated perfusion in partially fibrotic tissue samples (35.7 ± 5.2% of analyzed area) was 2.88 ± 0.18 $ml \cdot g^{-1} \cdot min^{-1}$, whereas measured MRI perfusion was only 1.86 ± 0.24 $ml \cdot g^{-1} \cdot min^{-1}$ ($P < 0.05$). These results indicate that resting perfusion in viable poststenotic myocardium is moderately reduced. Alterations in global and regional LV function are therefore secondary to both patchy fibrosis and reduced resting perfusion.

ischemic cardiomyopathy; necrosis

IN RATS WITH A CHRONIC coronary artery stenosis, regional and global left ventricular (LV) function is reduced (20), and the poststenotic myocardium is characterized by apoptosis and reparative fibrosis with normal myofibrillar ATPase activity (1, 8). Capasso et al. (8) observed that within the first 3 days following the induction of an ~60% diameter stenosis of a coronary artery, blood flow reserve was reduced whereas resting blood flow was normal in the poststenotic myocardium as measured using microspheres. However, quantitative data of poststenotic blood flow in the more chronic phase are lacking. In dogs and pigs with a chronic coronary artery stenosis and poststenotic contractile dysfunction, blood flow progressively decreases over weeks to months, possibly reflecting the progression of myocardium repetitively stunned into hibernation (6, 17). Whether such reduction in myocardial blood flow distal to a chronic coronary stenosis is caused by replacement fibrosis, and thus loss of viable tissue, or whether the perfusion in the remaining viable tissue is also reduced is not fully clear at present. Therefore, the first aim of the present study was to assess whether resting blood flow in the viable poststenotic tissue is reduced or remains normal. To assess regional myocardial blood flow and function at the same time, we used magnetic resonance (MR) imaging.

MATERIALS AND METHODS

Animal Model

The investigation conforms with the *Guide for the Care and Use of Laboratory Animals* published by the National Institutes of Health (NIH Publication No. 85-23, Revised 1996) and was approved by the local authorities. Experiments were carried out in adult female Wistar rats (Charles River, Sulzfeld, Germany) with a body weight of 250–300 g. Nonocclusive or occlusive coronary artery constriction of the anterior descending branch of the left coronary artery (LCA) was induced using methods described previously (7, 21). Briefly, a left thoracotomy was performed after intubation, and the pericardium was incised. Either the LCA was ligated, or a wire (300-μm diameter) was sutured to the vessel 2–3 mm from its origin and quickly removed thereafter. Thirty-seven to forty percent of the animals died within 24 h after surgery. In sham-operated rats, the ligation around the LCA was not tied and no animal died after surgery.

Experimental Preparation

For MR measurements in vivo, the animals received an initial dose of propofol (Disoprivan 2%, 100 mg/kg ip; Glaxo Wellcome, Bad Oldesloe, Germany) and were intubated and ventilated. Artificial ventilation was established with a small animal respirator (BAS-7025; FMI). The respirator was controlled using the pulse program of the MR spectrometer. Respiration of the animal was automatically stopped for ~4 s during image acquisition to avoid respiratory motion artifacts. The ECG trigger signal was received via foreleg electrodes, and heart rate was derived from a specially adapted ECG unit (Rapid Biomedical, Würzburg, Germany). The animals were positioned on an electrically heated pad to maintain a constant body temperature (37 ± 1°C). Anesthesia was maintained using propofol (40 $mg \cdot kg^{-1} \cdot min^{-1}$) administered via a tail vein.

MR Imaging of Myocardial Perfusion

All images were acquired on a 7.05 T Biospec 70/21 spectrometer (Bruker, Ettlingen, Germany). A specially adapted double-probehead for rat heart measurements was used, including a whole body coil for

Address for reprint requests and other correspondence: C. Waller, Universitätsklinik Würzburg, Medizinische Klinik, Josef-Schneider-Strasse 2, 97080 Würzburg, Germany (E-mail: waller_c@medizin.uni-wuerzburg.de).

The costs of publication of this article were defrayed in part by the payment of page charges. The article must therefore be hereby marked "*advertisement*" in accordance with 18 U.S.C. Section 1734 solely to indicate this fact.

transmission and a circular polarized surface coil as receiver (Rapid Biomedical).

Images were obtained in a short-axis slice perpendicular to the long axis of the left ventricle, which was identified after axial and long-axis scout views were obtained. The imaging slice was located 4–6 mm below the valvular plane, and slice thickness was 3 mm (Fig. 1*A*). For quantitative T_1 measurements, an inversion recovery snapshot fast, low-angle shot (FLASH) sequence was performed (15). Twenty-four diastolic-triggered snapshot FLASH images were acquired [repetition time (TR) 2.25 ms, echo time (TE) 1 ms, flip angle ~3°, slice thickness 3 mm], each within one heart cycle (180–200 ms). The image matrix was 64 × 64, zero filled to 128 × 128, resulting in a spatial resolution in plane of 310 × 310 μm^2 [field of view (FOV) 40 × 40 mm]. Time resolution of the T_1 measurement was improved by the measurement of two successive ECG-triggered T_1 experiments with different delays (varying in steps of ~80 ms) between the inversion pulse and the first FLASH image. Therefore, total acquisition time for one T_1 image was in the range of 2 × 24 = 48 FLASH images (1–2 min). Quantitative T_1 maps were gained by calculating T_1 for each pixel using a single-exponential fit from the time course of the measured signals (11). Further methodical details are described elsewhere (3, 28).

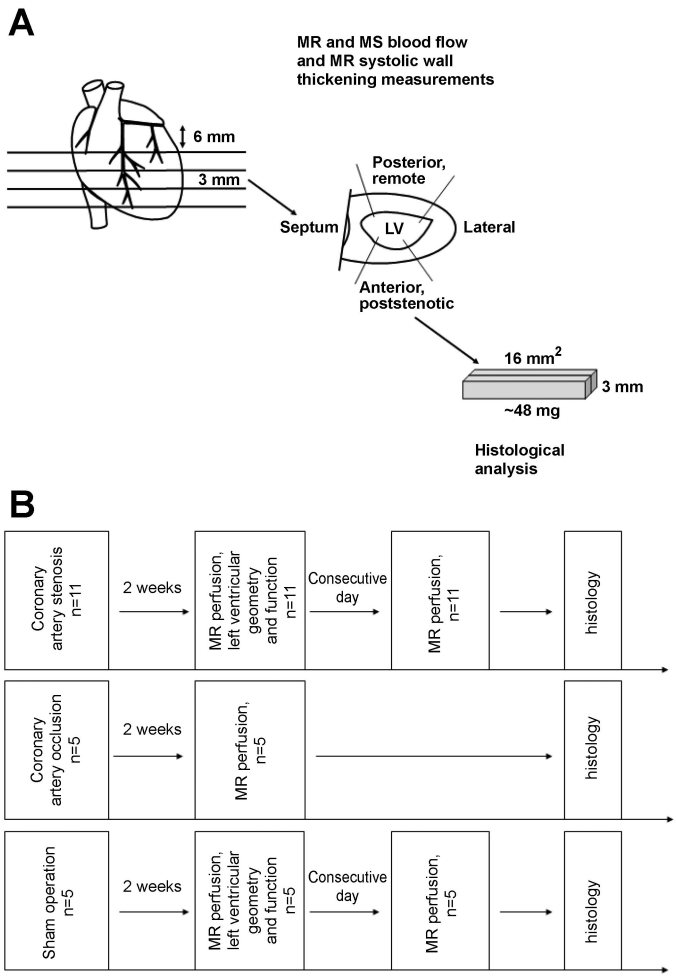

Fig. 1. *A*: scheme of tissue preparation. LV, left ventricular; MR, magnetic resonance; MS, microspheres. *B*: experimental protocol for all animal groups (coronary artery stenosis, sham, and coronary artery occlusion) from the time of operation to histology.

MR Imaging of Regional and Global LV Geometry and Function

An ECG-triggered fast gradient echo sequence was used with the following parameters: flip angle 30–40°, TE 1.1 ms, TR 3.2 ms, and 12 frames per heart cycle. The total acquisition time for one cine sequence was 40–50 s, depending on heart rate. The acquisition window per frame was 6.2 ms (2× TR). The acquisition matrix was 128 × 128, resulting in a spatial resolution in plane of 310 × 310 μm^2 (FOV 40 × 40 mm). To increase the signal-to-noise ratio, the images were averaged four times. For quantitative determination of the geometry and function, 16–20 contiguous ventricular short-axis slices of 1-mm thickness were acquired to cover the entire heart, resulting in a total acquisition time of ~20–30 min, depending on heart rate.

Data Analysis

Perfusion imaging. In the animals with coronary stenosis, regions of interest (ROI) of the left ventricle were defined by a manually drawn line. One region represented the poststenotic region in the anterior myocardial wall (40–60 pixels). The second region included the remote myocardium (150–210 pixels), and the third and fourth regions included the septal and the lateral myocardium, respectively (Fig. 1*A*). In sham rats, midmyocardial ROIs of the left myocardium comparable to those in the animals with coronary stenosis were manually delineated. Mean values for perfusion were obtained by averaging the pixel data in the ROI.

Cine imaging. Using an operator-interactive threshold technique, we determined myocardial and ventricular slice volumes from end-diastolic (largest LV diameter) and end-systolic (smallest LV diameter) images by multiplication of the compartment area and slice thickness (1 mm). Total volumes were calculated as the sum of all slice volumes. For LV mass measurement, epicardial and endocardial borders of all slices were delineated and the mass was defined as the volume within the borders multiplied by a factor of 1.05, which represents the myocardial specific density (g/cm^3). The papillary muscles were included in the traced area. Absolute cavity volumes were calculated in end diastole (EDV) and end systole (ESV) as the sum of all blood pool areas. Stroke volume (SV) and ejection fraction (EF) were calculated as follows: SV = EDV − ESV, and EF = SV/EDV. Cardiac output (CO) was determined as SV × HR. Myocardial wall thickness was measured in the remote region of the LV wall and in the poststenotic region in the end-diastolic (EDW) and end-systolic frame (EDW), and systolic wall thickening was calculated as a percentage: (ESW − EDW)/EDW.

Microsphere perfusion imaging. The noninvasive MR imaging spin-labeling technique allows the quantitative determination of myocardial perfusion (2, 3). In rat hearts in vivo, perfusion values measured by MR correlate to perfusion values measured with colored microspheres (28). However, whether MR is also able to quantify myocardial perfusion adequately in areas with reduced blood flow distal to a chronic coronary stenosis is unknown at present. Therefore, regional myocardial blood flow was also quantified on the day after the MR imaging measurements were obtained by using radiolabeled microspheres (MS measurements). Animals were anesthetized with ketamine (4 mg/100 g) and xylazine (1.5 mg/100 g) by intramuscular injection. Both anesthetics used in this study have been shown to result in comparable values for mean arterial blood pressure (MABP) and heart rate (HR) (26). The left femoral artery was cannulated (PE-50) for arterial blood sampling and for monitoring MABP and HR. A tracheotomy was performed, and animals were ventilated with a small animal respirator. MABP and HR were continuously monitored and recorded via the femoral artery with the use of a micromanometer (Millar Instruments, Houston, TX). Anesthesia was maintained by repeated intraperitoneal injections of ketamine and xylazine.

A left lateral thoracotomy was performed, and the pericardium was opened. Radiolabeled microspheres (15-μm diameter: ^{141}Ce, ^{113}Sn, and ^{103}Ru; NEN DuPont, Boston, MA) were injected within 5 s into

the left ventricle (4×10^5 spheres suspended in 0.2 ml of saline). The reference samples were collected from the arterial catheter beginning immediately before the injection of microspheres and continuing for 2 min. A total of 2 ml of blood was withdrawn at a rate of 1 ml/min with the use of a constant withdrawal pump (model 901A; Harvard Apparatus, Holliston, MA). The procedure used for the determination of blood flow has been described elsewhere (24).

Tissue Sampling and Morphometry

The entire heart was divided into three slices in the short-axis view (thickness ~3–5 mm). Each slice was cut into four tissue samples (anterior, lateral, septal, and posterior myocardial wall) with an average tissue sample size of 47 ± 2 mg (Fig. 1*A*). Normally perfused tissue contained ~1,000 spheres/sample, and hypoperfused tissue contained ~200 spheres/sample. The middle slice, which approximately covered the MR imaging slice, was used for further evaluations.

In a subset of seven rats with chronic coronary stenosis, after the radioactivity was counted in each probe, tissue samples were fixed in 6% formaldehyde for 24 h and then dehydrated and embedded in paraffin. Four sections of 2–4 μm in thickness were stained with hematoxylin and eosin and were analyzed with a microscope (Carl Zeiss, Göttingen, Germany) equipped with imaging software (Visitron Systems, Puchheim, Germany). Sections were quantitatively analyzed by two independent investigators for the volume fractions of the fibrotic lesions at a calibrated magnification of ×2.5. Mean total tissue area of the analyzed sections was 16.5 ± 1.4 mm^2.

Experimental Protocols

MR and MS measurements were performed in 11 animals with 2-wk coronary artery stenosis. MR measurements of perfusion and LV geometry and function were performed at rest. MS measurements were performed in the same animals on the following day. Finally, tissue samples were used for histological staining. In five sham-operated animals, MR and MS perfusion and cine imaging were performed for comparison with data from the animals with coronary stenosis. In five animals with 2-wk transmural myocardial infarction and fibrosis, MR perfusion was determined to quantify perfusion in scar tissue (Fig. 1*B*).

Statistical Analysis

The data are expressed as means ± SE. Data were regarded as different when two-tailed *P* values in *t*-tests were <0.05. With the use of Bland-Altman blot analysis (4), the agreement between MR and MS perfusion was calculated. Also, a linear regression between MR and MS perfusion was calculated and compared with the line of identity by using analysis of covariance (ANCOVA). In addition, a linear correlation between the fibrotic area (as a percentage of analyzed area) and MR perfusion in the poststenotic area (as a fraction of remote myocardium) was determined. This regression line was compared, using ANCOVA, with one based on measured blood flow data in totally fibrotic and normal sham myocardium. Finally, a linear regression analysis between the poststenotic regional myocardial blood flow (expressed as a percentage of regional myocardial blood flow in the remote area) and the poststenotic systolic wall excursion (expressed as a percentage of systolic wall excursion in the remote myocardium) was performed.

RESULTS

MR Imaging

A significant increase in LV mass and EDV was found in animals with chronic coronary artery stenosis. EF was significantly reduced in animals with chronic coronary artery stenosis compared with that in sham animals, whereas CO remained unaltered. Quantitative analysis of regional myocardial function revealed a decreased systolic wall thickening of the poststenotic segment of 18 ± 3% compared with 80 ± 7% in the remote region ($P < 0.001$). The HR of rats with a coronary artery stenosis was 286 ± 12 beats/min during MR imaging, which was comparable to HR obtained in sham animals (253 ± 15 beats/min) and in rats with complete coronary artery occlusion (268 ± 12 beats/min) (Table 1).

Quantitative perfusion data obtained by MR imaging of the animals with coronary stenosis showed a significant reduction to 2.21 ± 0.30 $ml \cdot g^{-1} \cdot min^{-1}$ in the poststenotic myocardium compared with that in the remote myocardium (4.05 ± 0.50 $ml \cdot g^{-1} \cdot min^{-1}$, $P = 0.02$). MR perfusion in the sham-operated animals was 3.80 ± 0.21 $ml \cdot g^{-1} \cdot min^{-1}$ in the anterior myocardium and 3.49 ± 0.23 $ml \cdot g^{-1} \cdot min^{-1}$ in the remote myocardium. MR perfusion data from the animals with transmural myocardial infarction revealed a significant reduction of 1.16 ± 0.14 $ml \cdot g^{-1} \cdot min^{-1}$ in the scar tissue vs. 3.85 ± 0.34 $ml \cdot g^{-1} \cdot min^{-1}$ in the remote myocardium ($P < 0.001$).

MS Perfusion Data

The HR of rats with a coronary artery stenosis was 229 ± 15 beats/min during MS perfusion measurement and 214 ± 23 beats/min in sham animals. The MABP of rats with a coronary artery stenosis was 104 ± 7 mmHg during MS perfusion measurement and 112 ± 9 mmHg in sham animals. Mean MS perfusion was 2.11 ± 0.31 $ml \cdot g^{-1} \cdot min^{-1}$ in the poststenotic area and 3.85 ± 0.36 $ml \cdot g^{-1} \cdot min^{-1}$ in the remote myocardium ($P < 0.01$). MS perfusion data from the sham animals show a mean perfusion of 4.49 ± 0.55 $ml \cdot g^{-1} \cdot min^{-1}$ in the anterior poststenotic wall and 4.11 ± 0.35 $ml \cdot g^{-1} \cdot min^{-1}$ in the remote myocardium.

There was a close correlation between MR and MS measurements of blood that was not different from the line of identity (Fig. 2*A*). Bland-Altman analysis confirmed the agreement between both methods (Fig. 2*B*).

Analysis of MR Perfusion and Function Distal to Coronary Stenosis

Samples taken from the poststenotic myocardium of the animals with coronary artery stenosis had an average fibrosis of 35.7 ± 5.2%. Linear regression analysis of MR blood flow relative to the extent of the fibrotic area is shown in Fig. 3. The upper line represents MR perfusion data from the completely fibrotic tissue of the animals with transmural myocardial infarction, with a perfusion of 32 ± 5% of the remote area, and MR perfusion data from the remote region as a fraction of

Table 1. *Magnetic resonance cine data*

Groups	Coronary Stenosis	Sham
HR, beats/min	286±12	253±15
BW, g	275±4	283±6
LV mass, mg	602.1±17.8*	518.5±22.9
LVEDV, μl	295.3±34.6*	183.2±17.1
SV, μl	135.3±8.8	135.8±5.4
EF, %	51.5±4.8*	69.3±4.3
CO, ml/min	46.3±5.1	40.9±2.4

Values are means ± SE. HR, heart rate; BW, body weight; LV, left ventricular; EDV, end-diastolic volume; SV, stroke volume; EF, ejection fraction; CO, cardiac output. *$P < 0.01$, coronary stenosis vs. sham.

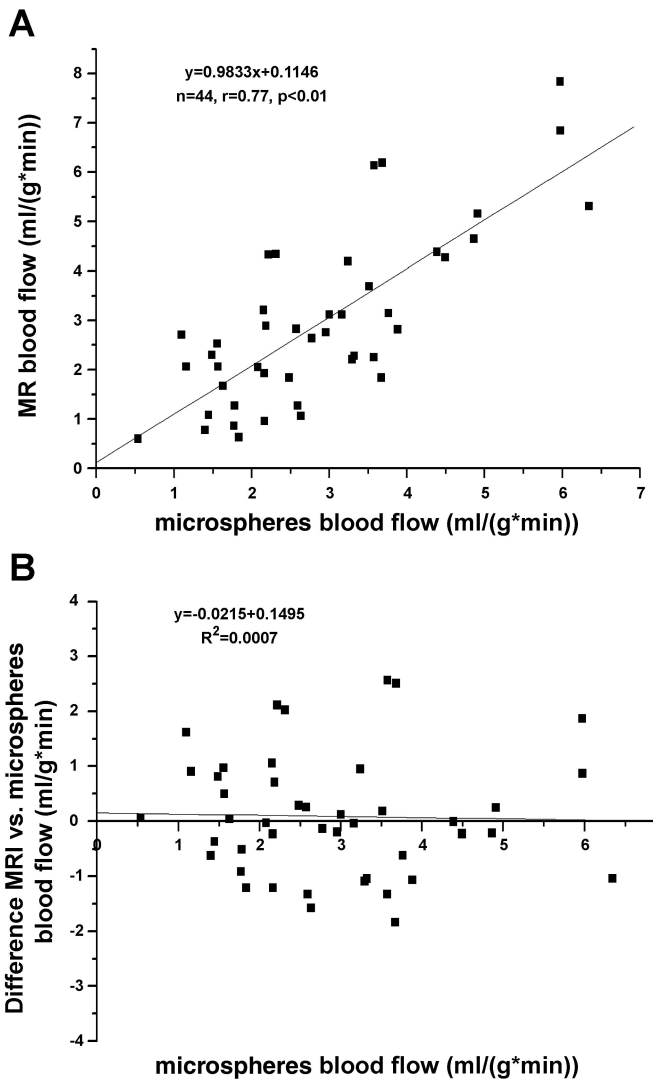

Fig. 2. *A*: linear regression analysis of both methods (MR and MS) for perfusion quantification. Corresponding myocardial regions show a close correlation of perfusion values obtained by MS or MR imaging (MRI) that was not different from the line of identity. *B*: Bland-Altman analysis confirms the agreement between both methods.

perfusion in sham animals with completely normal myocardium (114 ± 25%). The lower regression line was derived from MR poststenotic perfusion data, expressed as a percentage of the remote myocardium, relative to the fibrotic area, expressed as a percentage of the total tissue area, of animals with coronary artery stenosis. Both lines are significantly different from each other.

Systolic wall thickening in the four (septal, anterior, lateral, and posterior) regions of the left ventricle was 77.5 ± 14.1, 20.8 ± 6.7, 54.7 ± 11.7, and 93.0 ± 11.6%, respectively ($P <$ 0.01, posterior vs. anterior wall excursion). A significant relationship between the poststenotic perfusion (expressed as a percentage of perfusion in the remote area, *x*-axis) and the poststenotic systolic wall excursion (expressed as a percentage of systolic wall excursion in the remote myocardium, *y*-axis) was calculated (Fig. 4), suggesting that reduced perfusion is of importance for the reduced regional myocardial function. No

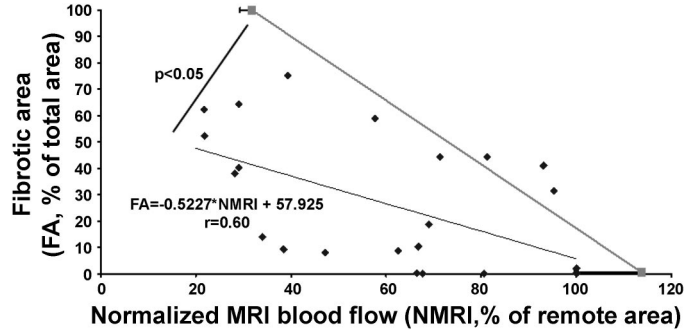

Fig. 3. Linear regression analysis of the infarcted area expressed as a percentage of the total area and the relative MRI flow reduction in the same tissue sample. *Upper line*: MRI perfusion resulting from data in completely fibrotic tissue of animals with transmural myocardial infarction and from data in the remote myocardium expressed as a fraction of perfusion in the normal myocardium of the sham animals. *Lower line*: MRI perfusion data of animals with coronary artery stenosis. FA, fibrotic area; NMRI, normalized MRI.

significant correlation was found between the extent of fibrosis and segmental wall thickening.

DISCUSSION

The small animal models of chronic coronary artery stenosis in rats and mice are widely used as experimental models of acute and chronic ischemia (7, 9, 20, 21). As in previous studies in large animals and humans (13, 14, 17, 22), blood flow to viable portions of poststenotic myocardium in rodents is reduced, as indicated in the present study. We showed that in the rat heart, poststenotic MR perfusion was significantly reduced, with a good correlation between MR perfusion and MS blood flow. The linear regression analysis of poststenotic MR perfusion relative to the amount of fibrotic tissue revealed reduced perfusion compared with the regression line of calculated perfusion. This calculated regression line assumes perfusion in the remote myocardium to be 114 ± 25% of that measured in normal myocardium of sham-operated rats and to be 32 ± 5% in pure scar tissue, as measured in animals with complete coronary occlusion and transmural infarction.

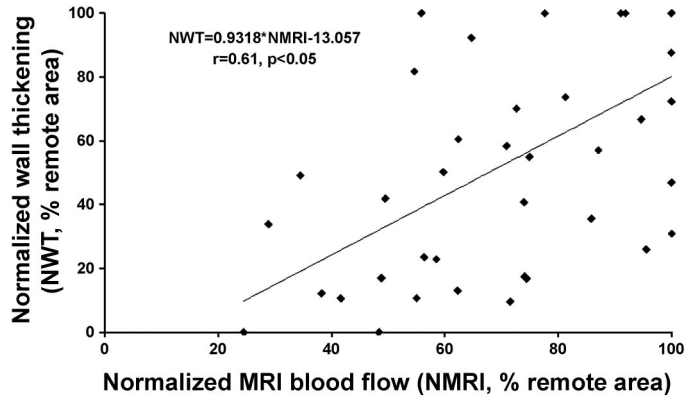

Fig. 4. Linear regression analysis between the poststenotic MRI perfusion (expressed as a percentage of regional myocardial blood flow in the remote area; *x*-axis) and the poststenotic systolic wall excursion (expressed as a percentage of systolic wall excursion in the remote myocardium; *y*-axis). NWT, normalized wall thickening.

Quantification of MR Perfusion vs. MS Perfusion

Recently, a noninvasive MR imaging technique was implemented for the quantification of myocardial perfusion in vivo (3). By using magnetic spin labeling of endogenous water protons, perfusion can be determined noninvasively without the use of additional contrast media. In intact beating rat hearts, validation studies have been performed using colored microspheres (17, 28). MR imaging has also been used to quantify perfusion in the remote myocardium during LV remodeling postmyocardial infarction (27). In the present study, MR imaging was used to detect perfusion in areas with reduced blood flow distal to a coronary stenosis in the rat heart. A good correlation close to the line of identity was found between blood flow data derived from both MR and MS measurements, even though measurements were performed on consecutive days. In addition, our data are in good accordance with perfusion data published by other groups (15, 24). MR imaging is therefore suitable to measure perfusion in poststenotic myocardium, even if tissue samples are partially fibrotic (35.7 ± 5.2% of the analyzed area in our study).

Perfusion in Viable Poststenotic Tissue in Rat Heart

Apart from the methodological validation, the second aim of our study was to determine whether a reduced poststenotic perfusion is caused by loss of viable tissue and/or by a decreased perfusion in the remaining viable myocardium. In a study by Capasso et al. (8), MS perfusion data obtained from rats 3–5 days after coronary stenosis revealed that the impairment of LV function was accompanied by a preserved resting and decreased maximal blood flow. Perfusion data obtained at later time points are available only for larger animal models. In pig hearts, resting perfusion distal to a fixed coronary stenosis was significantly reduced compared with remote myocardium after 1–8 mo. Such myocardium, which is characterized by a small increase in fibrosis, displayed a reduced function (14) and reduced regional oxygen consumption (19). In the present study, fibrosis in the poststenotic myocardium was more pronounced (36%) compared with that in the above-mentioned pig model (6%), potentially explaining the more pronounced decrease in poststenotic myocardial blood flow. However, late in the pig model and also in the present model, the decrease in blood flow was more closely related to the decrease in function than to the changes in morphology (for review, see Ref. 17). Also in humans, hibernating myocardium is characterized by an increase in myocardial fibrosis (12, 25). However, whether such poststenotic flow reduction is caused by tissue loss and replacement fibrosis or whether perfusion in the viable poststenotic tissue is also reduced remains controversial (5). Our study revealed that 2-wk coronary artery stenosis in rats induces the loss of ~36% of viable tissue. We demonstrated that perfusion in scar tissue determined by MR imaging was ~32% of the remote myocardium, confirming the results of others (10). Linear regression analysis allowed us to then distinguish alterations in perfusion due to viable tissue loss from that in the remaining poststenotic viable myocardium. A significant difference was shown to exist between the calculated and the measured perfusion in the poststenotic area, indicating that resting perfusion in viable poststenotic myocardium is reduced. In addition, the reduction of poststenotic MS perfusion correlated with the decline of poststenotic systolic wall thickening. Phenomenologically, our findings are consistent with hibernating myocardium, as was originally proposed by Rahimtoola et al. (22), although the final proof, recovery of function after revascularization, is not feasible in rats. However, we cannot determine from our data whether the reduced resting perfusion developed from repetitive stunning, although our data in conjunction with those of Capasso et al. (8), who found normal flow but reduced flow reserve after 3 days of stenosis, would suggest so.

Study Limitations

Ideally, flow and function should be measured at baseline and during the time course of the experimental protocol to normalize changes in flow and function occurring after the induction of coronary stenosis within a given piece of myocardium (poststenotic or remote) to the respective baseline values. However, such sequential measurements of flow and function were not obtained in the present study.

When measuring blood flow only once at the end of the experimental protocol (as done in the present study), MR and MS blood flow measurements should ideally be obtained at the same time to avoid alterations in confounding factors (e.g., HR, LV pressure). However, because legal and technical restrictions required that MR and MS measurements had to be obtained on consecutive days, we decided to normalize blood flow in the poststenotic area to that in the remote control area to partially account for variations in confounding factors. Therefore, part of the effect seen in the poststenotic area may be due to alterations within the remote area. However, HR (MRI: 219 ± 7 and 215 ± 7 beats/min vs. MS: 229 ± 15 and 214 ± 23 beats/min), and thus remote myocardial blood flow (MRI: 4.05 ± 0.50 $ml \cdot g^{-1} \cdot min^{-1}$ vs. MS: 3.85 ± 0.36 $ml \cdot g^{-1} \cdot min^{-1}$), on the consecutive days varied <5%.

In conclusion, there is good agreement between MR imaging and MS perfusion data in poststenotic myocardium in rats. Resting flow in poststenotic myocardium is reduced. Reduced perfusion is due not only to loss of viable tissue but also to reduced resting flow in viable myocardium, consistent with hibernation.

ACKNOWLEDGMENTS

We gratefully acknowledge the expert technical assistance of Yvonne Vogt, Sabine Voll, and Brigitte Schmitt.

GRANTS

This work was supported by the Deutsche Forschungsgemeinschaft (WA 1573/1-1 and SFB 355 A8) and by a grant from the Interdisziplinäres Zentrum für Klinische Forschung Würzburg (Teilprojekt F9, No. 01 KS-9603).

REFERENCES

1. **Anversa P, Malhotra A, Zhang X, Li P, Scheuer J, and Capasso JM.** Long-term coronary stenosis in rats: cardiac performance, myocardial morphology, and contractile protein enzyme activity. *Am J Physiol Heart Circ Physiol* 263: H117–H124, 1992.
2. **Bauer WR, Hiller KH, Galuppo P, Neubauer S, Köpke J, Haase A, Waller C, and Ertl G.** Fast high-resolution magnetic resonance imaging demonstrates fractality of myocardial perfusion in microscopic dimensions. *Circ Res* 88: 340–346, 2001.
3. **Belle V, Kahler E, Waller C, Rommel E, Voll S, Hiller KH, Bauer WR, and Haase A.** In vivo quantitative mapping of cardiac perfusion in rats using a noninvasive MR spin-labeling method. *J Magn Reson Imaging* 8: 1240–1245, 1998.

4. **Bland JM and Altman DG.** Measuring agreement in method comparison studies. *Stat Methods Med Res* 8: 135–160, 1999.
5. **Camici PG, Wijns W, Borgers M, De Silva R, Ferrari R, Knuuti J, Lammertsma AA, Liedtke AJ, Paternostro G, and Vatner SF.** Pathophysiological mechanisms of chronic reversible left ventricular dysfunction due to coronary artery disease (hibernating myocardium). *Circulation* 96: 3205–3214, 1997.
6. **Canty JM Jr and Fallavollita JA.** Resting myocardial flow in hibernating myocardium: validating animal models of human pathophysiology. *Am J Physiol Heart Circ Physiol* 277: H417–H422, 1999.
7. **Capasso JM, Jeanty MW, Palackal T, Olivetti G, and Anversa P.** Ventricular remodeling induced by acute nonocclusive constriction of coronary artery in rats. *Am J Physiol Heart Circ Physiol* 257: H1983–H1993, 1989.
8. **Capasso JM, Li P, and Anversa P.** Nonischemic myocardial damage induced by nonocclusive constriction of coronary artery in rats. *Am J Physiol Heart Circ Physiol* 260: H651–H661, 1991.
9. **Capasso JM, Malhotra A, Li P, Zhang X, Scheuer J, and Anversa P.** Chronic nonocclusive coronary artery constriction impairs ventricular function, myocardial structure, and cardiac contractile protein enzyme activity in rats. *Circ Res* 70: 148–162, 1992.
10. **Connelly CM, Leppo JA, Weitzman PW, Vogel WM, and Apstein CS.** Effect of coronary occlusion and reperfusion on myocardial blood flow during infarct healing. *Am J Physiol Heart Circ Physiol* 257: H365–H374, 1989.
11. **Deichmann R and Haase A.** Quantification of T_1 values by Snapshot-FLASH NMR imaging. *J Magn Reson* 96: 608–612, 1992.
12. **Elsasser A, Schlepper M, Zimmermann R, Muller KD, Strasser R, Klovekorn WP, and Schaper J.** The extracellular matrix in hibernating myocardium—a significant factor causing structural defects and cardiac dysfunction. *Mol Cell Biochem* 186: 147–158, 1998.
13. **Fallavollita JA, Malm BJ, and Canty JM Jr.** Hibernating myocardium retains metabolic and contractile reserve despite regional reductions in flow, function, and oxygen consumption at rest. *Circ Res* 92: 48–55, 2003.
14. **Fallavollita JA, Perry BJ, and Canty JM Jr.** ^{18}F-2-deoxyglucose deposition and regional flow in pigs with chronically dysfunctional myocardium. Evidence for transmural variations in chronic hibernating myocardium. *Circulation* 95: 1900–1909, 1997.
15. **Haase A.** Snapshot FLASH MRI. Application to T_1, T_2 and chemical-shift imaging. *Magn Reson Med* 13: 77–89, 1990.
16. **Hagendorff A, Dettmers C, Danos P, Pizzulli L, Omran H, Manz M, Hartmann A, and Luderitz B.** Myocardial and cerebral hemodynamics during tachyarrhythmia-induced hypotension in the rat. *Circulation* 90: 400–410, 1994.
17. **Heusch G.** Hibernating myocardium. *Physiol Rev* 78: 1055–1085, 1998.
18. **Heusch G and Schulz R.** Hibernating myocardium: new answers, still more questions! *Circ Res* 91: 863–865, 2002.
19. **Mills I, Fallon JT, Wrenn D, Sasken H, Gray W, Bier J, Levine D, Berman S, Gilson M, and Gewirtz H.** Adaptive responses of coronary circulation and myocardium to chronic reduction in perfusion pressure and flow. *Am J Physiol Heart Circ Physiol* 266: H447–H457, 1994.
20. **Nahrendorf M, Hiller KK, Greiser A, Köhler S, Neuberger T, Hu K, Waller C, Albrecht M, Neubauer S, Haase A, Ertl G, and Bauer WR.** Chronic coronary artery stenosis induces impaired function of remote myocardium: MRI and spectroscopy study in rat. *Am J Physiol Heart Circ Physiol* 285: H2712–H2721, 2003.
21. **Pfeffer MA, Pfeffer JM, Fishbein MC, Fletcher PJ, Spadaro J, Kloner RA, and Braunwald E.** Myocardial infarct size and ventricular function in rats. *Circ Res* 44: 503–512, 1979.
22. **Rahimtoola SH.** The hibernating myocardium. *Am Heart J* 117: 211–221, 1989.
23. **Schneider HJ, Pfeiffer D, and Hagendorff A.** The influence of bradycardia and normofrequent ventricular pacing on myocardial blood flow and energy demand in rats. *Cardiology* 100: 67–72, 2003.
24. **Schulz R, Miyazaki S, Miller M, Thaulow E, Heusch G, Ross J Jr, and Guth BD.** Consequences of regional inotropic stimulation of ischemic myocardium on regional myocardial blood flow and function in anesthetized swine. *Circ Res* 64: 1116–1126, 1989.
25. **Schwarz ER, Schoendube FA, Kostin S, Schmiedtke N, Schulz G, Buell U, Messmer BJ, Morrison J, Hanrath P, and vom Dahl J.** Prolonged myocardial hibernation exacerbates cardiomyocyte degeneration and impairs recovery of function after revascularization. *J Am Coll Cardiol* 31: 1018–1026, 1998.
26. **Shiga Y, Minami K, Uezono Y, Segawa K, Nagaoka E, Shiraishi M, Noguchi T, and Shigematsu A.** Effects of the intravenously administered anaesthetics ketamine, propofol, and thiamylal on the cortical renal blood flow in rats. *Pharmacology* 68: 17–23, 2003.
27. **Waller C, Hiller KH, Kahler Hu K E, Nahrendorf M, Voll S, Haase A, Ertl G, and Bauer WR.** Serial magnetic resonance imaging of microvascular remodeling in the infarcted rat heart. *Circulation* 103: 1564–1569, 2001.
28. **Waller C, Kahler E, Hiller KH, Hu K, Nahrendorf M, Voll S, Haase A, Ertl G, and Bauer WR.** NMR in vivo assessment of myocardial perfusion and intracapillary blood volume in rats at rest and coronary dilation. *Radiology* 215: 189–197, 2000.